



## Article

# Switching Order after Failures in Symmetric Protective Electrical Circuits with Triple Modal Reservation

Anton O. Belousov <sup>1,2,\*</sup> , Artem V. Medvedev <sup>1</sup>, Evgeniya B. Chernikova <sup>1</sup> , Talgat R. Gazizov <sup>1,2</sup> and Alexander M. Zabolotsky <sup>1</sup>

<sup>1</sup> Television and Control Department, Tomsk State University of Control Systems and Radioelectronics, 634050 Tomsk, Russia; medart20@rambler.ru (A.V.M.); chiernikova96@mail.ru (E.B.C.); talgat@tu.tusur.ru (T.R.G.); zabolotsky\_am@mail.ru (A.M.Z.)

<sup>2</sup> Sirius University of Science and Technology, 354340 Sochi, Russia

\* Correspondence: ant1lafleur@gmail.com; Tel.: +7-(923)-440-86-02

**Abstract:** This work is devoted to the research of new asymmetry effects in symmetric protective structures with triple modal reservation. We analyzed the structures with different cross-sectional locations of the reference conductor: in the center (unshielded structure), around (shielded structure), at the top and bottom (multilayer printed circuit board), and in the form of side polygons (double-sided printed circuit board). First, a preliminary quasi-static simulation was performed in the range of parameters. It was revealed that in all structures, except for the shielded one (in the form of a cable), the deviations of the output voltage amplitude, bandwidth, and frequency of the first resonance were insignificant, whereas in the shielded structure there were significant deviations in the time and frequency responses. The attenuation of the output voltage in relation to the input for each structure was also estimated. In addition, we performed a parametric optimization of the structures under consideration using a heuristic search, which made it possible to improve their characteristics. Finally, the switching order between the conductors in these structures with the original and optimized parameter sets was investigated in detail. The optimal conductor switching order in the case of a component failure was determined, and the best (according to protective characteristics) parameter configuration for each structure was found.

**Keywords:** electromagnetic compatibility; intentional electromagnetic interference; ultrashort pulse; protective devices; multiconductor transmission lines; redundancy; modal reservation; switching order; component failure



**Citation:** Belousov, A.O.; Medvedev, A.V.; Chernikova, E.B.; Gazizov, T.R.; Zabolotsky, A.M. Switching Order after Failures in Symmetric Protective Electrical Circuits with Triple Modal Reservation. *Symmetry* **2021**, *13*, 1074. <https://doi.org/10.3390/sym13061074>

Academic Editor: Albert Ferrando

Received: 28 April 2021

Accepted: 11 June 2021

Published: 16 June 2021

**Publisher's Note:** MDPI stays neutral with regard to jurisdictional claims in published maps and institutional affiliations.



**Copyright:** © 2021 by the authors. Licensee MDPI, Basel, Switzerland. This article is an open access article distributed under the terms and conditions of the Creative Commons Attribution (CC BY) license (<https://creativecommons.org/licenses/by/4.0/>).

## 1. Introduction

With the growth of technical progress, the complexity of radioelectronic equipment (REE) increases and exacerbates the problem of ensuring the necessary reliability of systems and components. Despite all the measures (including manufacturing the most advanced devices based on the most cutting-edge technologies), the reliability of components cannot keep up with the growing system complexity. Comparing the requirements that have been imposed on REE earlier and today, it is possible to establish the reasons for both continuous system complication and their relatively low reliability. It is also easy to understand why system complexity far outstrips the one that would be appropriate according to the rate of component development. The issue lies in balancing between what we have and what we need. We need complex devices now. This is the requirement of scientific and technological progress. One of the ways to resolve this contradiction is to introduce hardware redundancy or reservation [1,2]. The significance of reservation for ensuring high device reliability can be explained by examples from nature. It is reservation or redundancy to which extremely complex and, at the same time, highly reliable devices—living organisms—owe their existence. One of the main redundancy types is structural redundancy or, in a simpler way, reservation. As soon as the problem of ensuring the reliability and safety of rather

complex or unreliable devices emerges, then one, if not the only, solution is reservation. Its purpose is to provide the smooth operation of REE even in the case of failure of one or more of its parts. This may be the most cost-effective or perhaps the only solution if reliability requirements are beyond the state-of-the-art technology level. However, the pay for reservation, in addition to the increase in complexity, cost, size, and weight of REE, is a significant increase in power consumption, as well as the complication of the equipment check and maintenance. If the reason for the failure can affect all the REE reserving elements at the same time, then the benefits of reservation will be lost [3,4]. A well-known way to increase reliability for partially maintained or unattended REE is cold reservation. In the case of a failure of the reserved (or primary) circuit, the power is supplied to the reserving (or the secondary) one, which was not previously used. When a reserved circuit is operating, the reserving one is not used and has almost no effect on its operation. If the reserved circuit fails, the switching device switches the power supply to the reserving circuit [5,6]. The main parameter of reservation is its multiplicity factor—the ratio of the number of reserving (secondary) devices to the number of reserved (primary) ones [7]. Therefore, multiple reservation is used in cases where it is necessary to ensure high reliability [8]. However, the multiplicity of reservation is limited by weight, dimensions, and cost.

Meanwhile, the increasing complexity of modern REE leads to the aggravation of another important problem—the assurance of electromagnetic compatibility (EMC) [9,10]. The relevance of ensuring EMC and increasing the REE noise immunity in particular is high. This is caused by the widespread use of REE in various fields of technology. Another reason is EMC concerns all structural levels of the equipment: from microchips to onboard REE [11,12]. Special attention should be paid to the increase in the speed and packaging density of modern REE, which makes it extremely susceptible to the effects of both external and internal electromagnetic interference (EMI). There are several reported cases of intentional EMI excitations on REE that entailed negative consequences [13,14]. Particularly dangerous is the conducted interference of an ultrashort pulse (USP), which has a high voltage level and nanosecond rise time, in contrast to other types of intentional EMI. Despite the low USP energy, the effectiveness of its impact on a conventional system can be significant. Experimental studies have confirmed that the measure of the induced energy is not the total pulse duration, but its energy in a certain frequency interval that is critical for a specific device [15].

Protecting equipment from an interfering USP is a difficult task. The existing traditional protection devices do not often provide adequate protection since the response time of many protection devices exceeds the USP duration, passing it to the critical REE nodes [16,17]. In this regard, it is worth noting the structures operating on the principle of modal filtration, called modal filters (MF), which were previously proposed for REE protection against USPs. They do not have the disadvantages of traditional protection devices. In an MF, during the propagation of a pulse excited in an active conductor of a line segment (with a non-uniform dielectric filling) consisting of  $N$  conductors (not counting the reference), it can undergo modal distortions. This can entail the decomposition into  $N$  pulses of smaller amplitude due to the difference in the per-unit length delays of the line modes [18]. It is remarkable that MF-based protection may not require a protection device, as it uses the existing printed circuit board (PCB) connections.

Nowadays, it is important to develop reliable systems that are immune to electromagnetic interference [19]. In REE with reservation, both reliability and EMC assurance, in terms of radiated susceptibility and conducted emissions, depend on the location of the reserving conductors relative to each other [20–22]. There is a single modal reservation (MR) (duplication) and a multiple MR, the multiplicity factor of which is greater than one. Methods of single, double, and triple MR have been proposed. With a double MR, three modes arrive at the structure output, and with a triple MR, four modes. Meanwhile, a triple MR implies the use of four-conductor structures with a symmetrical conductor arrangement to increase the modal filtration efficiency with MR.

Note that the authors recently investigated the influence of symmetry and asymmetry of a number of protective structures in which modal phenomena take place [18]. Recently, two fundamentally new MF configurations were proposed [23]. They are a conventional microstrip line with one or two conductors on top that are grounded at both ends of the line. Noteworthy are the differences in the characteristics of the proposed MF from the known ones. First, the minimum and equal pulse voltages at the output of the known MFs, as a rule, are obtained with loads at the ends of the passive conductor, the values of which are equal to the geometric mean of the mode wave impedances, and in some MFs, with a short circuit (SC) at one end and open circuit (OC) at the other. However, in the new MFs, equal pulse voltages are obtained when a passive conductor is short-circuited at both ends of the reference one. Secondly, many known MFs have a symmetrical (or close to it) arrangement of active and passive conductors relative to the reference, which ensures the equality of pulse voltage amplitudes. However, in the new MFs, this is ensured with a sharply asymmetric arrangement of these conductors relative to the reference one. In this case, one of the MFs has two passive conductors rather than one, which are located symmetrically relative to the reference one. Finally, among the subsequent pulses, there are additional pulses with delays equal to linear combinations of the pulse mode delays.

However, in these studies, only one very specific aspect of asymmetry effects was considered in detail: the appearance of additional pulses in the time response to the USP excitation. Meanwhile, simpler influences on initially symmetric structures, which lead to their asymmetry, have not been investigated. An example is the influence of the geometric parameter variation on the per-unit length mode delays in the structure or on its time and frequency responses. Such research is relevant because it determines a change in important protection characteristics. The examples for the time response are the maximum duration of the USP, which will decompose completely, and its attenuation coefficient. For the frequency response, examples include the bandwidth, which is important for undistorted transmission of the useful signal, and the frequency of the first resonance, where the maximum attenuation will take place.

In addition, preliminary studies of triple MR structures have shown that because of the difference in couplings between conductors, the switching order will be important. So, for instance, in the case of a failure simulated either by an SC or by an OC at one of the ends of the reserved circuit, the switch to the reserving circuit changes the maximum voltage of the decomposition pulses at the structure output. In a simple example (double reservation) of a conventional microstrip line of three conductors, where conductor 1 is reserved (or primary) and conductors 2 and 3 are reserving (or secondary), if conductor 1 (active) fails, conductor 2 (passive) will replace it and become active itself. However, the geometric parameters of the cross-section can be such that the choice of conductor 3, and not 2, as the first reserving conductor will provide a greater attenuation of the exciting USP at the output of the device. Therefore, it is advisable to correctly and efficiently switch between the conductors.

The theoretical and practical groundwork accumulated in the field of MR, along with the available tools for the symmetric structures research, allows us for the first time to start solving problems arising while investigating the structures with a triple MR. Based on the above, it is possible to highlight the main innovation of this research, which consists of a systematic examination of the optimal conductor switching order in symmetric structures with a triple MR after failure. This study seems to be significant and relevant, especially considering that the implementation of this order does not require any additional costs. To generalize the application of such technical solutions to typical areas, one can study structures with different cross-sectional locations of the reference conductor: in the center (unshielded structure), around (shielded structure), at the top and bottom (multilayer PCB), and in the form of side polygons (double-sided PCB). It is worth considering the optimal switching order in these structures for two sets of parameters: before and after optimization. It is useful to apply these approaches when solving the following tasks:

- to simulate the structure in the range of parameters;

- to determine the optimal switching order after failures;
- to identify the best parameter configuration (before or after optimization) in terms of protective features after failures.

The aim of this paper is to present the results of such research.

## 2. Approaches and Methods

To achieve this aim, a multivariate analysis of time and frequency responses was used in the range of cross-section (for structures without failures) and equivalent circuit (for structures with failures) parameters. It was assumed that T-waves are propagating along the structures under consideration. Initially, cross-section geometric models of the structures were constructed. Next, the per-unit-length coefficient matrices of electrostatic ( $C$ ) and electromagnetic ( $L$ ) inductances were calculated, and on their basis, the matrices of characteristic impedance ( $Z$ ) and per-unit-length mode delays ( $\tau_i$ ) were calculated. Losses in the structures were not taken into account in order to eliminate their influence at this stage of research. To calculate the responses, we created a schematic diagram to simulate each structure, and set loads and electromotive force (EMF) values, followed by the calculation of the time and frequency responses in the range of parameters. Failures in the structures under consideration were simulated either by an SC or an OC. The quasi-static simulation based on the method of moments was carried out in the TALGAT software [24], where the above models and steps were implemented.

Parametric optimization of structures without failure was performed. Because of the structure symmetry, the number of optimized parameters was restricted. For example, changing the width of individual conductors will violate the structure symmetry. In addition, the experience of practical optimization of protective structures makes it possible to determine with high accuracy the degree to which the optimized parameters impact the output voltage waveforms (especially in symmetrical structures). Therefore, since the number of optimized parameters is limited and the available experience in practical simulation and optimization is considerable, there is no need to resort to time-consuming global optimization methods. Accordingly, parametric optimization of structures was carried out using heuristic search demonstrating positive results.

Optimization using heuristic search implies manual parameter enumeration, in which a sequential action order is repeated. It includes changing the values of the parameters of the structures under consideration, recording the results obtained, and analyzing them. In addition, it is important to determine the range in which the optimized parameters will change. For example, with 5 optimized parameters, a number of effective options for such optimization is possible: fixing 4 and changing 1 (option 1), fixing 3 and changing 2 (variant 2), or fixing 2 and changing 3 (variant 3) parameters. Fixing 1 and changing 4 parameters is not recommended since increased complexity of determining the individual parameter(s) affects the change in the structure output characteristics. Meanwhile, in protective structures, the optimization of which has not been performed before, it is recommended to use option 1 until it becomes clear which output characteristics of the optimized structures are affected by a change in individual parameters. Thus, when using option 1, the selected parameter increases from the lower range value or decreases from the upper one with a certain step. During the optimization, the fixed parameters are set equal to the average value of the optimization range. At the same time, attention is paid to the processes taking place in the optimized structure. In addition, the output characteristics that change as a result of such a search are recorded (for example, in the structure under consideration, a change in the width of the conductors in a certain way affects the amplitudes of the decomposition pulses and the value of the characteristic impedance). Then the next parameter is optimized, etc. When optimizing the structures under consideration, it is assumed that the optimization of the parameter values that have an immediate impact on the degree of electromagnetic coupling between conductors (due to the symmetry of the structures) is direct.

The rest of the article is structured as follows:

- Section 3 includes a multivariate analysis of the structures under consideration;
- Section 3.1 presents 4 structures with a triple MR for further research;
- Sections 3.2 and 3.3 cover the simulation and analysis results of the structures in the time and frequency domains;
- Section 3.4 presents the parametric optimization and analysis results;
- Section 4 includes subsections demonstrating simulation, selection, and evaluation of the optimal switching order of the active conductor in these structures after failures;
- Section 4.1 includes a description and analysis of circuits that simulate sequential failures at one end of the active conductor in the structures under consideration;
- Sections 4.2–4.5 systematize the results of examining the structures with a reference conductor in the center, around, above and below, and in the form of side polygons;
- Section 5 discusses the main results;
- Section 6 systematizes the results obtained and highlights the prospects for further work.

### 3. Multivariate Analysis of Structures with Triple Modal Reservation

#### 3.1. Structures under Consideration

We considered structures with a reference conductor in the center, around, above and below, and in the form of side polygons. Their cross-sections are shown in Figure 1, where  $w$  is the width of the conductors,  $w_1$  is the width of the side polygons,  $s$  is the separation between the conductors,  $t$  is the thickness of the conductors,  $h$  is the thickness of the dielectric,  $d$  is the distance from the edge of the structure to the conductor (for the structure with polygons it is the distance between the polygon and the signal conductor),  $r_c$  is the radius of the conductors,  $r_d$  is the radius of the dielectrics,  $r_r$  is the radius of the reference conductor, and  $\epsilon_r$  is the relative permittivity of the dielectric (in the structure with the reference conductor, the designations  $\epsilon_{r1}$  and  $\epsilon_{r2}$  are used to denote the relative permittivity of the different PCB layers). In these structures, the symmetry of the cross-sections and boundary conditions is maintained.

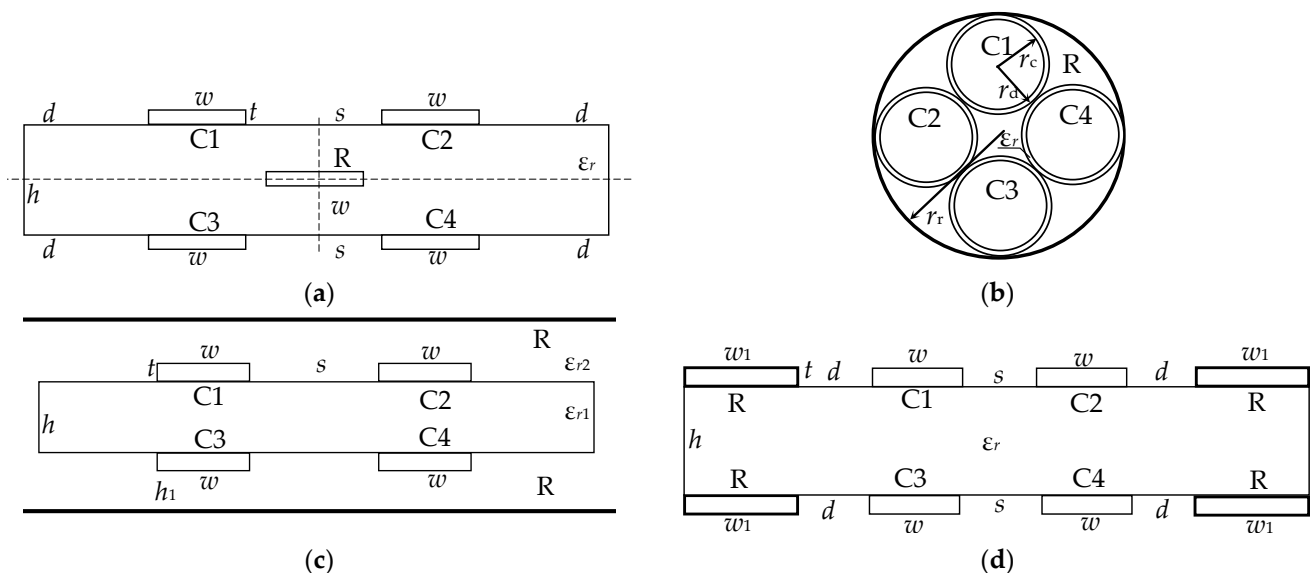


**Figure 1.** Cross-sections of structures with the reference conductor (a) in the center, (b) around, (c) above and below, and (d) in the form of side polygons, where conductor C1—active; C2, C3, C4—passive; and R—reference.

The structure with the reference conductor in the center (Figure 1a) is a symmetrical strip structure. In such a structure, due to the symmetry and location of the reference conductor, it is easy to provide pairwise equalized amplitudes of the decomposition pulses as well as equal time intervals between them. The structure with the reference conductor around (Figure 1b) is a shielded four-conductor insulated cable that is widely used in practice. The structure with the reference conductor at the top and bottom (Figure 1c) is a



shielded strip structure in the form of a multilayer PCB. In this structure, the broad-side coupling provides high attenuation values of the exciting USP and high differences in per-unit-length mode delays ( $\Delta\tau$ ). In addition, due to the presence of an external shield, this structure provides protection against radiated emissions. The structure with the reference conductor as side polygons (Figure 1d) is a strip structure acting as a double-sided PCB. This design simplifies its fabrication, packaging, and integration while maintaining the broad-side coupling, as in the structure in Figure 1c.

An equivalent circuit of the structures under study is shown in Figure 2a. The length of the strip structures was equal to  $l = 0.5$  m, and the shielded cable 1 m. As an excitation, we used an EMF source with a trapezoid pulse signal with an amplitude of 2 V. The durations of the rise, fall, and flat top (at levels 0–1) were equal to 50 ps, so the total duration was 150 ps (Figure 2b). The load values ( $R$ ) were chosen from the condition of matching the structure to the path (i.e., the signal amplitude at the beginning of the line ( $V_2$ ) should be equal to half of the EMF ( $V_1$ ) (Figure 2a) [18].

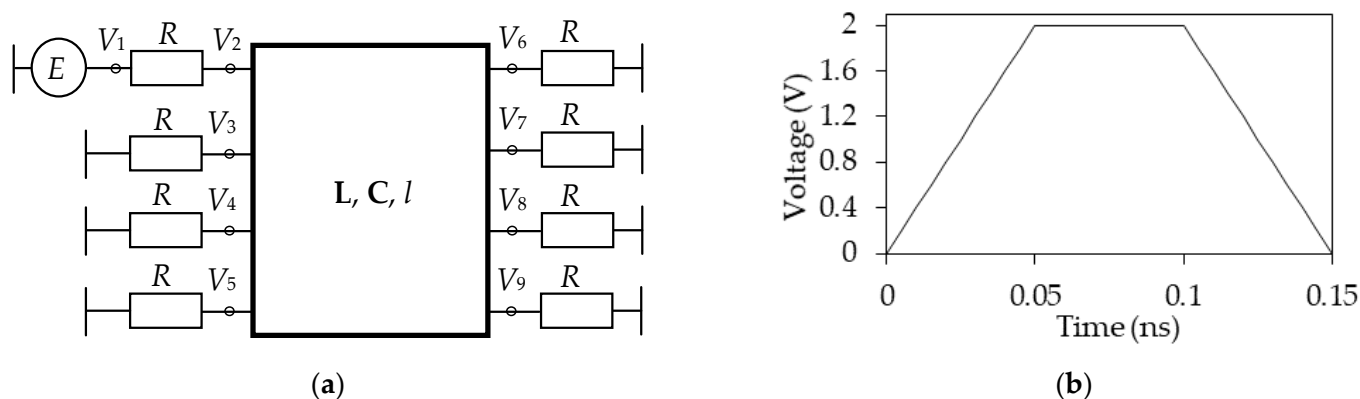


**Figure 2.** (a) Equivalent circuit of the structures under consideration and (b) EMF waveform.

A simulation of the time and frequency responses was carried out in the range of cross-sectional parameters with a small variation of their values relative to parameter set 1 (Tables 1 and 2). The main cross-section parameters are presented in three sets. This was primarily done to provide a thorough investigation, as well as to estimate the effect of the parameter value deviation from set 1 on the output characteristics.

**Table 1.** Cross-section parameter sets for strip structures.

Structure with a Reference Conductor	Parameter Sets	Parameter Values			
		$s, \mu\text{m}$	$w, \mu\text{m}$	$t, \mu\text{m}$	$h, \mu\text{m}$
In the center	1	400	300	105	300
	2	450	350	140	350
	3	350	250	70	250
Above and below	1	200	200	35	180
	2	250	250	70	200
	3	150	150	18	150
In the form of side polygons	1	510	1600	35	500
	2	550	1650	70	550
	3	450	1550	18	450

**Table 2.** Cross-section parameter set for shielded cable.

Structure with a Reference Conductor	Parameter Sets	Parameter Values		
		$r_c, \mu\text{m}$	$r_d, \mu\text{m}$	$r_t, \mu\text{m}$
Around	1	1500	1750	4350
	2	2000	2250	5500
	3	1000	1250	3100

### 3.2. Time Domain Analysis

Voltage waveforms at the output of the structures under study before optimization are presented in Figure 3. The maximum voltage values ( $U_{\max}$ ) and the values of  $\tau_i$ , calculated in the range of parameters, are summarized in Table 3 and presented in Section 3.2.

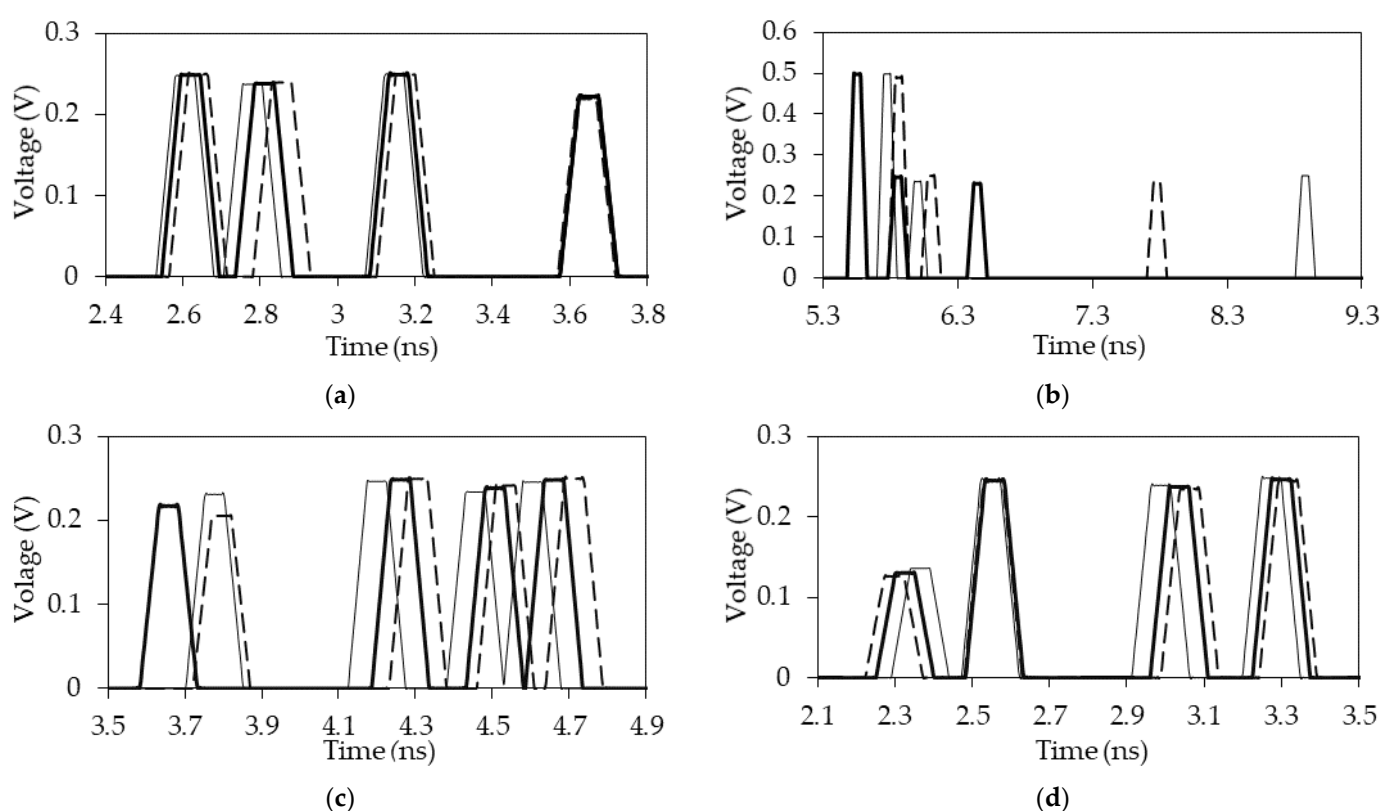


**Figure 3.** Output voltage waveforms for the structures with the reference conductor (a) in the center, (b) around, (c) above and below, and (d) in the form of side polygons with parameter sets 1 (—), 2 (---), and 3 (- -).

From Figure 3, it is seen that the use of parameter sets 2 and 3 had little effect on the  $\tau_4$  value in the structure with the reference conductor in the center, or on the  $\tau_2$  value in the structure with the reference conductor in the form of side polygons. At the same time, simulation in the range of the structural parameters with the reference conductor around (where, among other things, we can see the overlap of pulses 1 and 2), as well as above and below, showed different  $\tau_i$  values.

The maximum deviation values of  $\tau_1$ ,  $\tau_2$ ,  $\tau_3$ , and  $\tau_4$  for the structures (in the order of mention) were 0.034, 0.076, 0.028, and 0.01 ns/m; 0.31 (for pulses 1 and 2 that arrived at the same time), 0.24, and 2.435 ns/m; 0.138, 0.107, 0.083, and 0.108 ns/m; and 0.032, 0.012, 0.063, and 0.033 ns/m. The maximum difference between the  $\tau_i$  values was estimated by comparing the results obtained in simulations with three parameter sets. For the structure with the reference conductor in the center, this value was observed for pulse 2 (0.034 ns/m), around for pulse 3 (far right) (2.435 ns/m), above and below for pulse 1 (0.138 ns/m), and in the form of side polygons for pulse 3 (0.063 ns/m).

**Table 3.** Numerical characteristics of the structures under consideration after simulation.

Structure with a Reference Conductor	Parameter Sets	Parameters						
		$U_{\max}$ , V	$\tau_1$ , ns/m	$\tau_2$ , ns/m	$\tau_3$ , ns/m	$\tau_4$ , ns/m	$\Delta f$ , GHz	$f_1$ , GHz
In the center	1	0.2473	2.544	2.735	3.082	3.573	0.296	1.436
	2	0.2473	2.530	2.704	3.071	3.577	0.290	1.402
	3	0.2471	2.564	2.780	3.099	3.567	0.302	1.482
Around	1	0.4970	5.475	5.475	5.780	6.370	0.337	1.666
	2	0.4980	5.695	5.695	5.925	8.805	0.098	2.103
	3	0.4960	5.785	5.785	6.020	7.705	0.158	1.861
Above and below	1	0.2490	3.582	4.185	4.430	4.585	0.340	1.596
	2	0.2470	3.701	4.122	4.377	4.527	0.366	1.832
	3	0.2510	3.720	4.230	4.460	4.635	0.344	1.692
In the form of side polygons	1	0.2437	2.239	2.453	2.936	3.201	0.286	0.662
	2	0.2435	2.269	2.457	2.898	3.183	0.290	0.782
	3	0.2435	2.207	2.445	2.961	3.217	0.282	0.696

Nevertheless, with all parameter sets, the  $U_{\max}$  value remained practically unchanged for each structure. Thus, the structure with the reference conductor in the center can provide an attenuation relative to the input voltage level by 4.04 times, around by 2.01 times (this is explained by the superposition of pulses 1 and 2 because of the specificity of the electromagnetic coupling between the conductors), from above and below by 3.98 times, and in the form side polygon by 4.18 times.

### 3.3. Frequency Domain Analysis

The frequency responses at the output of the structures under study were also obtained for three sets of parameters and are presented in Figure 4. The bandwidth values at the level of 0.707 ( $\Delta f$ ) and the first resonance frequency ( $f_1$ ) for each structure are summarized in Table 3.

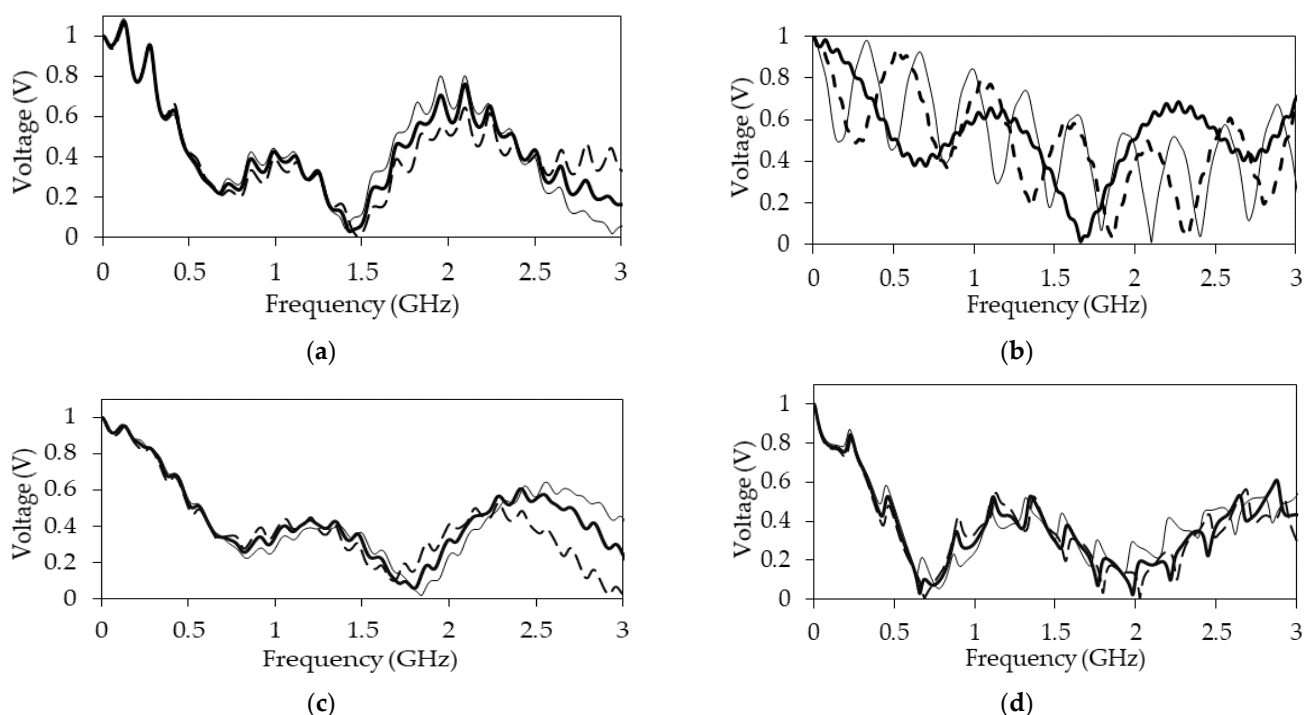


**Figure 4.** Frequency responses of structures with the reference conductor (a) in the center, (b) around, (c) above and below, and (d) in the form of side polygons with parameter sets 1 (—), 2 (---), and 3 (- -).



From Figure 4 and Table 3 it follows that the  $\Delta f$  values for structures with the reference conductor in the center and in the form of side polygons varied slightly for all sets of parameters; the difference did not exceed 0.012 GHz or 0.008 GHz for either structure, respectively. The  $f_1$  values for different sets of parameters also differed slightly (0.08 GHz and 0.12 GHz for parameter sets 1–3 for both structures, respectively). The  $\Delta f$  values for the structure with the reference conductor at the top and bottom differed for parameter set 2 relative to the others (the deviation was about 0.026 GHz). The  $f_1$  values for different sets of parameters of this structure also slightly differed (the maximum difference was 0.236 GHz between parameter sets 1 and 2). Meanwhile, for the structure with a reference conductor around, the  $\Delta f$  values differed in all parameter sets (the difference between parameter sets 1 and 2 was 0.239 GHz, between 1 and 3 was 0.179 GHz, and between 2 and 3 was 0.06 GHz). The  $f_1$  values for parameter sets 1–3 were also different (the maximum difference was 0.437 GHz between parameter sets 1 and 2).

### 3.4. Optimization

When optimizing the strip structures, the  $s$  and  $w$  values varied in the range of 50–2000  $\mu\text{m}$ ;  $t$  in the range of 18–175  $\mu\text{m}$ ,  $h$  in the range of 200–3000  $\mu\text{m}$ , and  $d$  in the range of 200–2000  $\mu\text{m}$ . The optimized cross-section parameters of the strip structures are presented in Table 4. When optimizing the shielded cable, the  $r_i$  values varied in the range of 200–4000  $\mu\text{m}$ . As a result of optimization, the following parameters were obtained:  $r_c = 900$   $\mu\text{m}$  (conductor C1),  $r_c = 800$   $\mu\text{m}$  (conductors C2 and C3),  $r_c = 700$   $\mu\text{m}$  (conductor C4),  $r_d = 970$   $\mu\text{m}$  (dielectric around C1),  $r_d = 950$   $\mu\text{m}$  (dielectric around C2, C3 and C4),  $r_r = 3500$   $\mu\text{m}$ ,  $\epsilon_r = 30$  (dielectric around C1),  $\epsilon_r = 5$  (dielectric around C2),  $\epsilon_r = 16$  (dielectric around C3), and  $\epsilon_r = 6$  (dielectric around C4). The voltage waveforms at the output of all structures after optimization are shown in Figure 5.

**Table 4.** Optimized parameters for strip structures.

Structure with a Reference Conductor	$s$ , $\mu\text{m}$	$w$ , $\mu\text{m}$	$h$ , $\mu\text{m}$	$t$ , $\mu\text{m}$	$d$ , $\mu\text{m}$
In the center	510	1600	500	18	1600
Above and below	200	260	100	135	6400
In the form of side polygons	220	500 ( $w_1 = 1600$ $\mu\text{m}$ )	300	18	800

After optimization, the  $U_{\text{max}}$  value for the structure with the reference conductor in the center did not change (before and after optimization—0.248 V) since the pairwise alignment of the amplitudes of pulses 1 and 3, and 2 and 4 (due to symmetry) was deliberately achieved. For the structure with a reference conductor at the top and bottom, the  $U_{\text{max}}$  value was 0.24 V (before optimization it was 0.25 V). Finally, for the structure with a reference conductor in the form of side polygons the  $U_{\text{max}}$  value was 0.235 V (before optimization it was 0.243 V).

In addition, for the three above-mentioned structures, it was possible to equalize the time intervals between the decomposition pulses so that the  $\Delta\tau_i$  values were 0.245, 0.255, and 0.245 ns/m; 0.34, 0.355, and 0.36 ns/m; and 0.255, 0.252, and 0.27 ns/m, respectively.

It should also be noted that it is much more difficult to achieve complete decomposition of the exciting USP in a shielded cable than in strip structures. This is due to the specific character of electromagnetic coupling between the conductors. Nevertheless, after optimization, the  $U_{\text{max}}$  value was 0.29 V (before optimization it was 0.5 V). The increased attenuation of the exciting USP was obtained by establishing different couplings between the C1–C2 and C1–C4 conductors. As a result, the amplitudes of pulses 1, 2, and 4 were equalized.

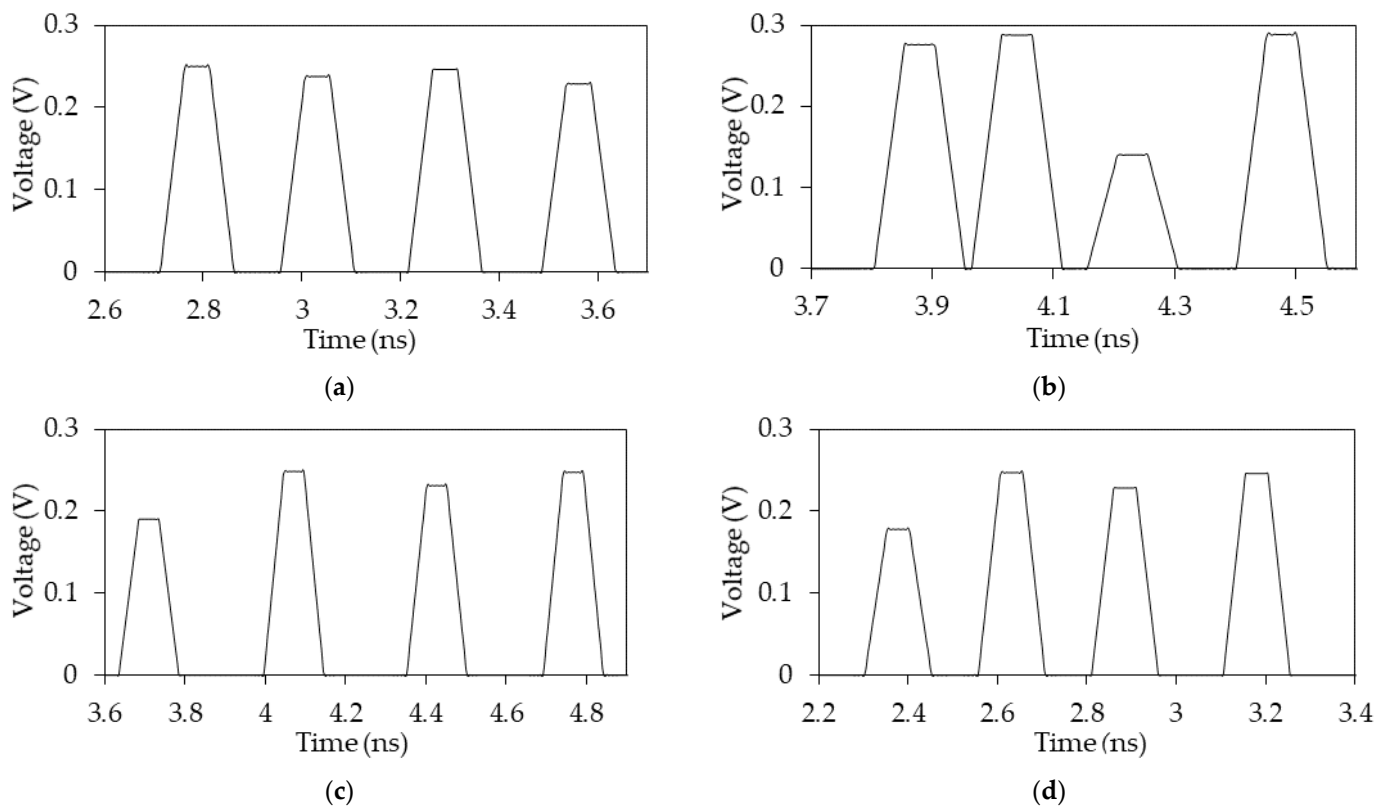


**Figure 5.** Voltage waveforms at the output of the structures with a reference conductor (a) in the center, (b) around, (c) above and below, and (d) in the form of side polygons after optimization.

#### 4. Simulation, Selection, and Evaluation of the Optimal Switching Order in Structures with Triple Modal Reservation

##### 4.1. Active Conductor Switching Options after Failures

Figure 6 shows the options for choosing an active conductor after sequential failures at one of the ends of the structures with a triple MR. Figure 7 shows an equivalent circuit that simulates sequential failures at one end of the active conductor. After failure 1, it is possible to switch to any of the three free conductors. In this case, the switching order determines the behavior of the output characteristics (the decomposition pulse amplitudes  $U_i$  and the  $\tau_i$  values). Thus, after failure 1, three switching options appear. After failure 2, for each of the three options, two switching options remain, and after failure 3, you can switch only to the last remaining conductor (Figure 6). Let us consider, for example, option 1 after failures (Figure 6, the extreme path on the left): After failure 1 at one of the active conductor C1 ends, we can switch to the conductor C2 and the output characteristics will change; after failure 2, we can switch to either C3 (option 1.1) or C4 (option 1.2). However, from Figure 1a it follows that the characteristics for these options will be the same. This is because the two remaining conductors are located on one conductive layer of the structure. After failure 3 for options 1.1 and 1.2, you can switch to either C4 or C3. However, in this case, the output characteristics will also be the same. Consequently, there are three switching orders; failure 3 does not affect the switching order (Figure 7) in the case of symmetrical structures. Figure 7 shows that C1 is the active conductor in each case (before and after faults). Moreover, each failed conductor was an active conductor before the failure, which is also true for all symmetric structures. Thus, the equivalent circuit shown in Figure 7 is valid for all symmetric structures with triple MR.

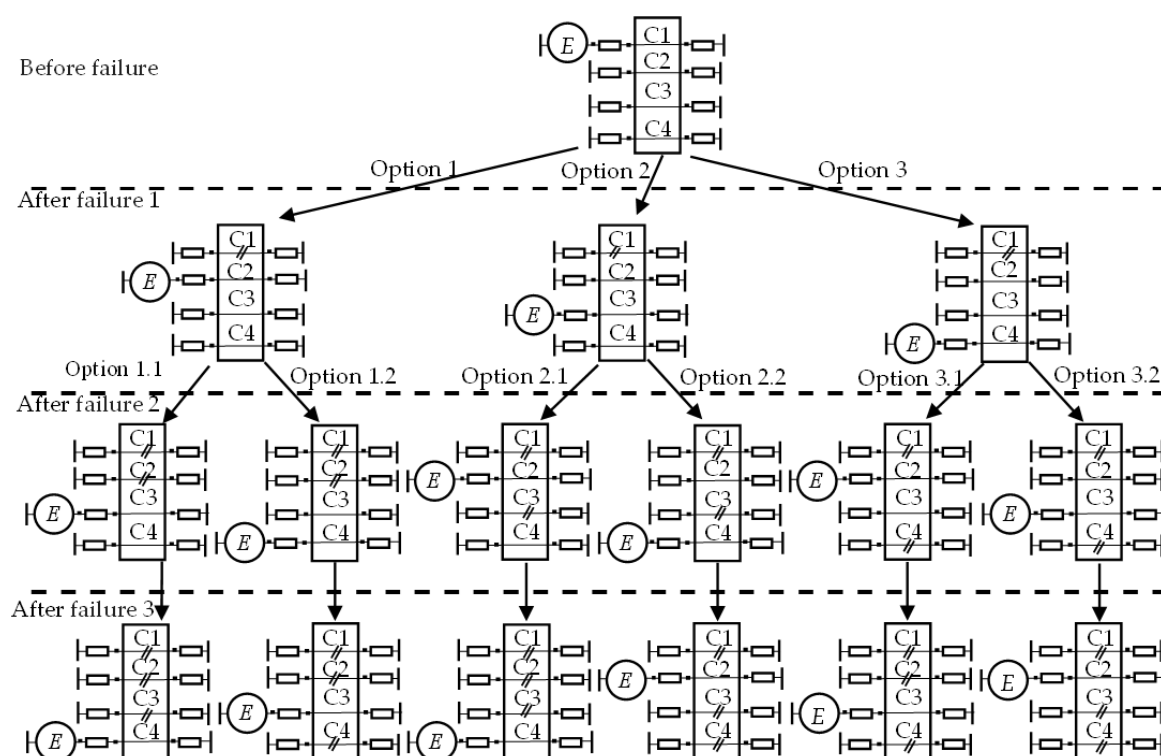


**Figure 6.** Options for selecting another active conductor after sequential failures at one end of the active conductor for a structure with triple MR.

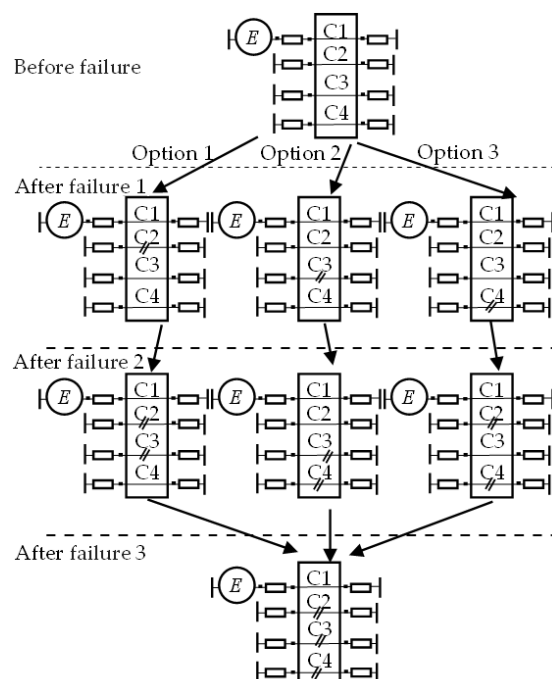


**Figure 7.** Equivalent circuit that simulates sequential failures at one end of the active conductor for symmetric structures with triple MR (each failed conductor is an active conductor before a failure).

#### 4.2. Structure with the Reference Conductor in the Center

A cross-section of a triple MR structure with the reference conductor in the center is shown in Figure 1a. For the simulation, the original and optimized sets of cross-sectional parameters were used, which are summarized in Table 5. The resistor  $R$  nominal was

chosen equal to  $92\ \Omega$  for the original parameter set, and  $50\ \Omega$  for the optimized one for the structure before failures. If the reserved circuit failed (SC or OC), it was assumed that the reserving circuit took over the functions of the reserved one. In the simulation, the values of resistors  $R1$  and  $R2$  for the active conductor were equal to  $R$  (i.e., the  $R$  values before failure). The nominal resistor values on passive conductors were equal to  $1\ \text{M}\Omega$  (OC), and  $1\ \mu\Omega$  (SC) for various failures.

**Table 5.** Parameter sets for simulation.

Set	$w$ , mm	$s$ , mm	$t$ , mm	$h$ , mm	$\epsilon_r$
Original	0.3	0.40	0.105	0.3	5
Optimized	1.6	0.51	0.018	0.5	4.5

For this structure, the voltage waveforms at the far end of the active conductor (C1) with the original parameter set after failures 1 and 2 are shown in Figures 8–12. Note that we only specified waveforms that were not identical for different failure options. So, for example, the waveforms with an active conductor C1 with  $R$ – $R$  (at the near–at the far ends at C2),  $R$ – $R$  (at the near–at the far ends at C3), and  $R$ – $R$  (at the near–at the far ends at C4) were identical to the forms of voltages with active conductors—C2, C3, and C4, respectively (Figure 7). In addition, the voltage waveforms were identical if the boundary conditions on the passive conductors for different failure options were symmetrical. For example, the voltage waveform of the  $R$ – $R$  option on C2,  $R$ – $SC$  on C3, and  $OC$ – $R$  on C4 was identical to  $R$ – $R$  on C2,  $SC$ – $R$  on C3,  $R$ – $OC$  on C4, respectively, etc. This was true for all considered parameter sets. Voltage waveforms with the minimum (best case) and maximum (worst case)  $U_{\max}$  values are presented below.

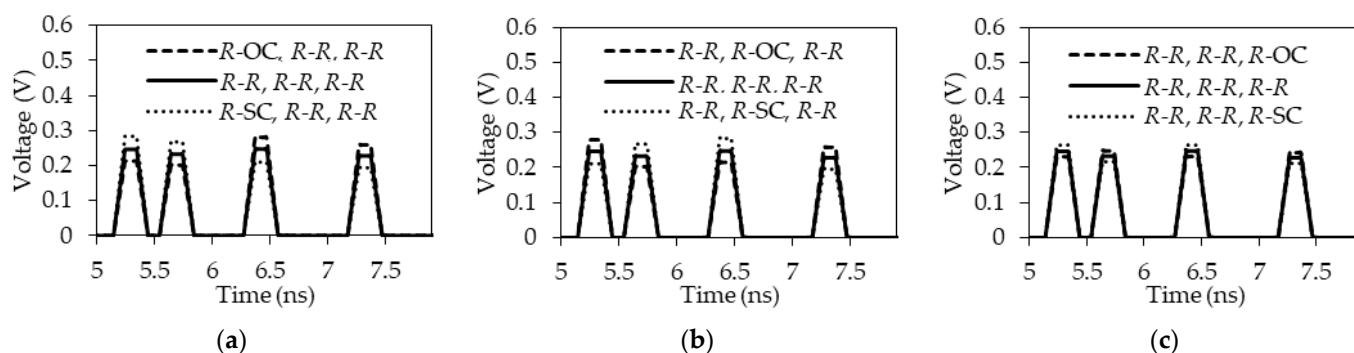


**Figure 8.** Voltage waveforms at the far end of C1 under different boundary conditions at the ends of (a) C2, (b) C3, and (c) C4 (after failure 1).

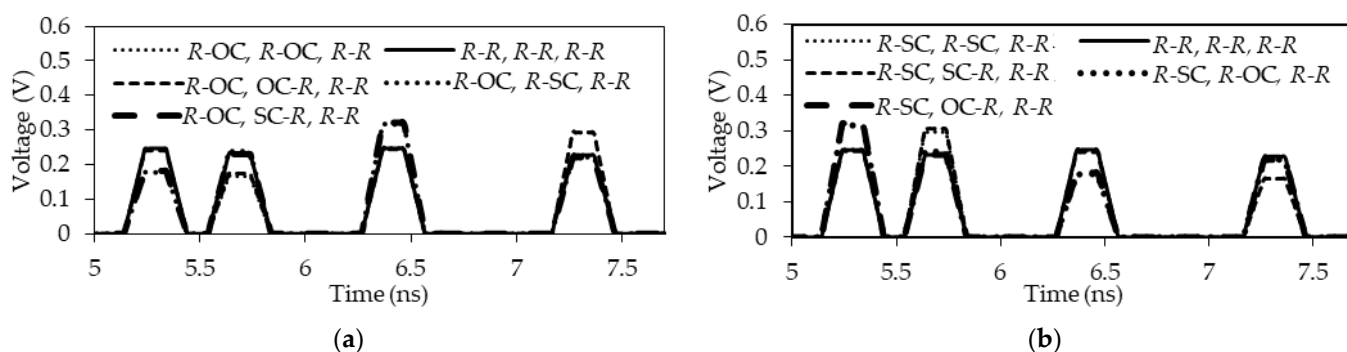


**Figure 9.** Voltage waveforms at the far end of C1 with (a) OC and (b) SC at the far ends of C2 and different boundary conditions at the end of C3 with option 1 (after failure 2).

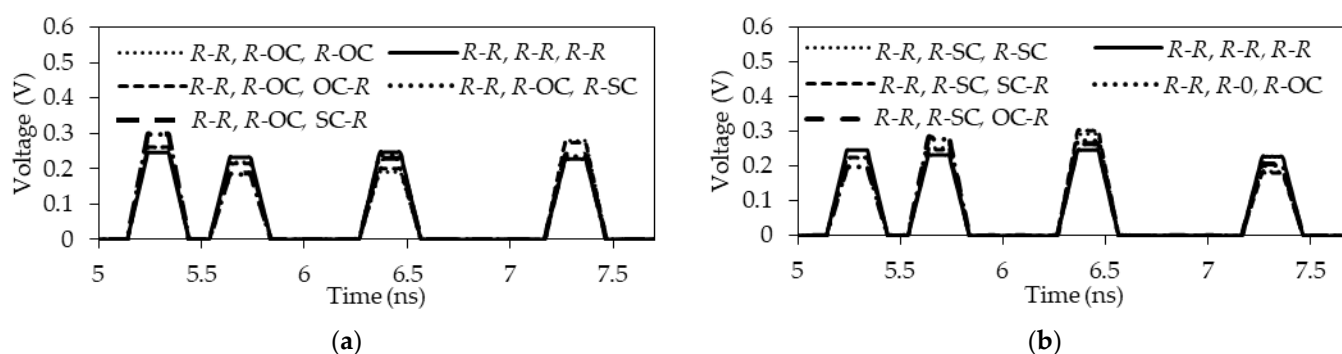


**Figure 10.** Voltage waveforms at the far end of C1 with (a) OC and (b) SC at the far end of C3 and different boundary conditions at the ends of C4, with option 2 (after failure 2).

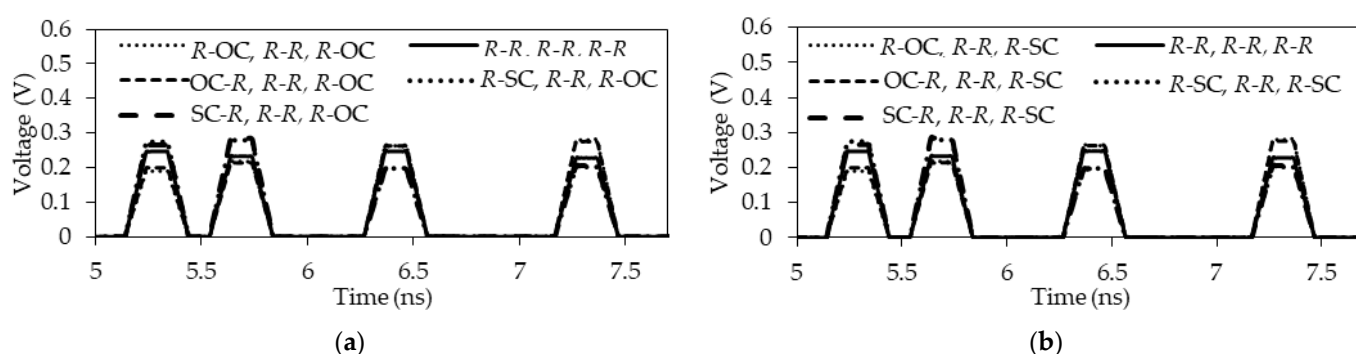


**Figure 11.** Voltage waveforms at the far end of C1 with (a) OC and (b) SC at the far end of C4 and different boundary conditions at the ends of C2, with option 2 (after failure 2).

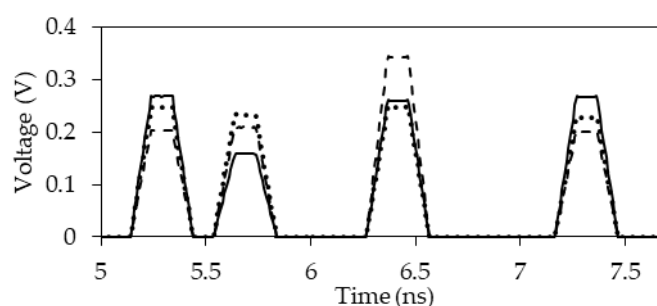


**Figure 12.** Voltage waveforms at the far end of C1 under boundary conditions at the ends of passive conductors for R-R, R-R, R-R (....), R-OC, OC-R, R-SC (—) and R-OC, SC-R, R-SC (—) (after failure 3).

From Figures 8–12 it can be seen that after failures 1, 2, and 3 (Figure 7), when the boundary conditions on the passive conductors C2, C3, and C4 changed, the amplitude values of each of the decomposition pulses changed. The figures shed light on these changes. In the rest of the paper, voltage waveforms are not considered. The  $U_{\max}$  values for structures with original and optimized parameter sets after failures 1, 2, and 3 are summarized in Table S1 (in Supplementary Materials). Figure 13 shows the dependences of  $U_{\max}$  values on the failure number for structures with original and optimized parameter sets.

Figure 13a shows that for the structure with the original parameter set, with switching options 1, 2, and 3, after failure 1 there was an increase in the  $U_{\max}$  value to 0.284, 0.285, and 0.266 V, respectively; after failure 2 to 0.324, 0.305, and 0.303 V, respectively; and after failure 3 to the same level of 0.346 V, which did not depend on the switching option. Switching option 3 is optimal, since the  $U_{\max}$  values after failures 1 and 2 were minimal (0.266 and 0.303 V, respectively).

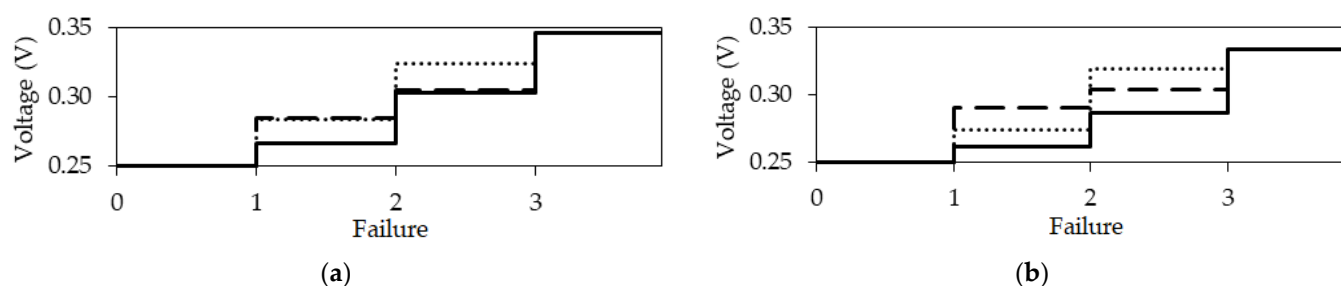


**Figure 13.** Dependences of  $U_{\max}$  values on the failure number with options 1 ( $\cdots$ ), 2 ( $---$ ), and 3 ( $—$ ) for the structure with (a) original and (b) optimized parameter sets.

Figure 13b shows that for the structure with the optimized parameter set, with switching options 1, 2, and 3, after failure 1 there was an increase in the  $U_{\max}$  value to 0.274, 0.29, and 0.262 V, respectively; after failure 2 to 0.319, 0.304, and 0.287 V, respectively; and after failure 3 up to 0.334 V. Switching option 3 is optimal, since the  $U_{\max}$  values after failures 1 and 2 were minimal (0.262 and 0.287 V, respectively). The  $U_{\max}$  values for the optimal switching orders are summarized in Table 6. Figure 14 shows the dependences of the  $U_{\max}$  values on the failure number for structures with the original and optimized parameter sets.

**Table 6.**  $U_{\max}$  values for optimal switching orders.

Set	Before Failure	$U_{\max}$ , V	After Failure 1	$U_{\max}$ , V	After Failure 2	$U_{\max}$ , V	After Failure 3	$U_{\max}$ , V
Original	R-R, R-R, R-R	0.250	R-R, R-R, R-SC	0.266	SC-R, R-R, R-SC	0.303	R-OC, SC-R, R-SC	0.346
Optimized	R-R, R-R, R-R	0.250	R-R, R-R, R-SC	0.262	SC-R, R-R, R-SC	0.287	R-SC, OC-R, SC-R	0.334

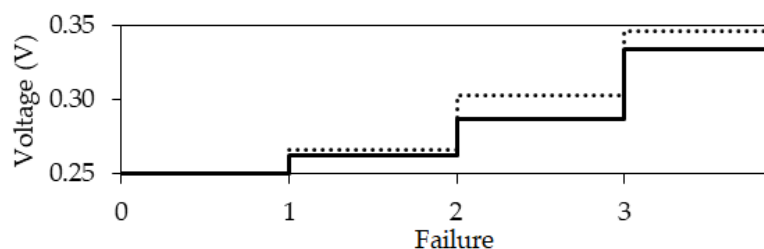


**Figure 14.** Dependences of  $U_{\max}$  values on the failure number at the optimal switching orders for the structure with the original ( $\cdots$ ) and optimized ( $—$ ) parameter sets.

Figure 14 shows that with the optimal switching orders after failure 1, there was an increase in  $U_{\max}$  value up to 0.266 (for the original parameter set) and 0.262 V (for the optimized parameter set). After failure 2, the increase went up to 0.303 and 0.287 V, respectively, and after failure 3 up to 0.346 and 0.334 V, respectively. Thus, with the optimized parameter set, the  $U_{\max}$  values after all failures were minimal and equal to 0.262, 0.287, and 0.334 V, respectively. Therefore, the optimized parameter set is more preferable in this case.

#### 4.3. Structure with the Reference Conductor Around

A cross-section for simulating a triple MR structure with a reference conductor around is shown in Figure 1b. The original and optimized cross-sectional parameter sets were used for this (Table 7). Note that the structure with a reference conductor around is the only one that, in the course of optimization, lost the cross-section symmetry for ensuring different electromagnetic couplings between conductors, and, as a consequence, complete decomposition of an exciting USP.



Table 7. Parameter sets for simulation.

Set	$r_c$ , mm				$r_d$ , mm (Around Conductors)				$r_r$ , mm	$\varepsilon_r$ (Around Conductors)			
	C1	C2	C3	C4	C1	C2	C3	C4		C1	C2	C3	C4
Original	1.50	1.50	1.50	1.50	1.75	1.75	1.75	1.75	4.35		10		
Optimized	0.90	0.80	0.80	0.70	0.97	0.95	0.95	0.95	3.50	30	5	16	6

In the simulation,  $R$  nominals were chosen equal to  $12\ \Omega$  for the original parameter set and  $31\ \Omega$  for the optimized one. The  $U_{\max}$  values for the structure with the original parameter set after failures 1, 2, and 3 are summarized in Table S2. Figure 15 shows the dependence of  $U_{\max}$  on the failure number for the structure with the original parameter set for switching options 1, 2, and 3 (from Table S2).

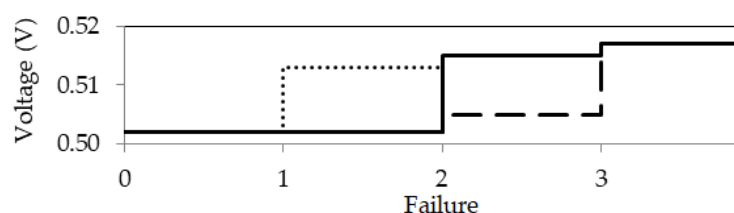


Figure 15. Dependences of  $U_{\max}$  values on the failure number at the switching options 1 ( $\cdots$ ), 2 ( $---$ ), and 3 ( $—$ ) for the structure with the original parameter set.

Figure 15 shows that for switching options 1, 2, and 3, after failure 1 there was an increase in the  $U_{\max}$  value to 0.513, 0.502, and 0.502 V, respectively. After failure 2 it went up to 0.515, 0.505, and 0.515 V, respectively, and after failure 3 up to 0.517 V. Thus, for this structure, switching option 2 is optimal since the  $U_{\max}$  values after failures 1 and 2 were minimal (0.502 and 0.505 V, respectively).

The  $U_{\max}$  values for the structure with the optimized parameter set after failures 1, 2, and 3 are summarized in Table S3. Figure 16 shows the dependence of the  $U_{\max}$  values on the number of the failure for the structure with the optimized parameter set. Since this structure lost its cross-sectional symmetry during the optimization, the circuit shown in Figure 6 was used to study the switching order. In this circuit, only the optimal switching order shown in Figure 17 was considered.

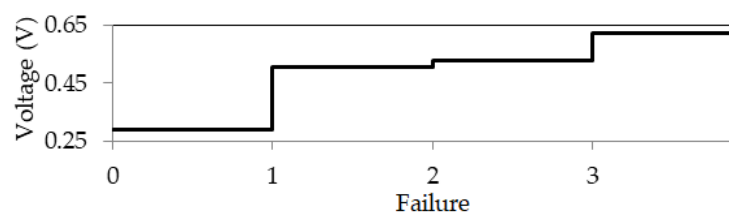
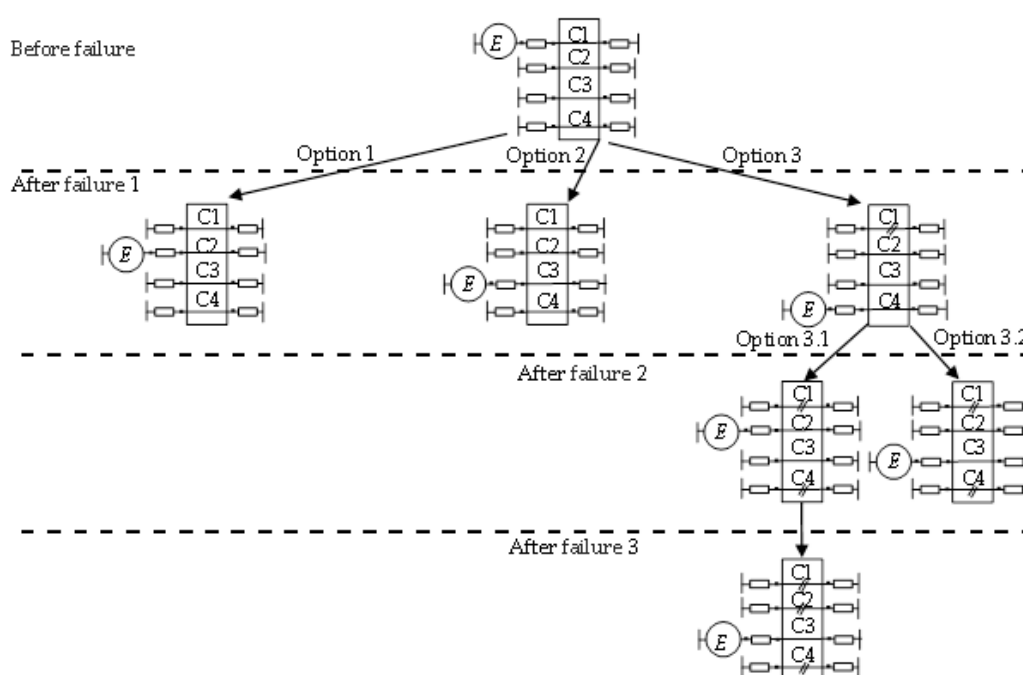


Figure 16. Dependence of  $U_{\max}$  for the optimal switching option from the failure number for a structure with an optimized parameter set.

Table S3 shows that for options 1, 2, and 3 after failure 1, there was an increase in  $U_{\max}$  up to 0.517, 0.766, and 0.507 V, respectively. After failure 2 it went up to 0.527 and 0.769 V, respectively, and after failure 3 up to 0.622 V. The optimal switching option is 3 since the  $U_{\max}$  values after failures 1 and 2 in this case were minimal (0.507 and 0.527 V, respectively), as can be seen in Figure 16). The  $U_{\max}$  values for the optimal switching orders are summarized in Table 8. Figure 18 shows the  $U_{\max}$  dependences (from Table 8) for the original and optimized parameter sets on the failure number.



**Figure 17.** Optimal switching order for active conductor after sequential failures at one of the ends of the active conductor for the structure with a triple MR with a reference conductor around.

**Table 8.**  $U_{\max}$  values for optimal switching orders.

Set	Before Failure	$U_{\max}$ , V	After Failure 1	$U_{\max}$ , V	After Failure 2	$U_{\max}$ , V	After Failure 3	$U_{\max}$ , V
Original	R-R, R-R, R-R	0.502	R-R, R-R, R-OC	0.502	R-R, R-SC, OC-R	0.505	R-OC, R-SC, R-SC	0.517
Optimized	R-R, R-R, R-R	0.291	R-R, R-R, R-SC	0.507	R-SC, R-R, SC-R	0.527	R-OC, R-SC, SC-R	0.622

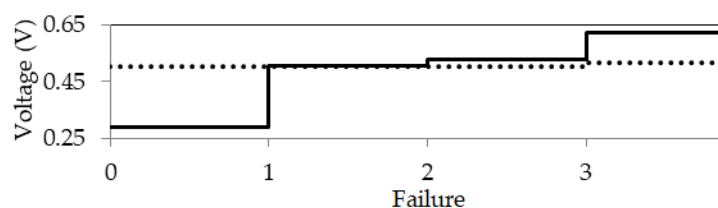


**Figure 18.** Dependences of  $U_{\max}$  values on the failure number for options 1, 2, and 3 for the structure with the original (···) and optimized (—) parameter sets.

Figure 18 shows that with optimal switching orders after failure 1, the  $U_{\max}$  value increased to 0.502 (for the original parameter set) and 0.507 V (for the optimized parameter set). After failure 2, the increase went up to 0.505 and 0.527 V, respectively, and after failure 3 up to 0.517 and 0.622 V, respectively. Thus, for the original parameter set, the  $U_{\max}$  values after all failures were minimal and equal to 0.502, 0.505, and 0.517 V, respectively. Therefore, the original parameter set is preferable.

#### 4.4. Construction with the Reference Conductor Above and Below

A cross-section for simulating a triple MR structure with the reference conductor above and below is shown in Figure 1c. The simulation was based on the original and optimized cross-section parameter set (Table 9). The  $R$  values (before failures) were equal to

40  $\Omega$  for the original set 1 and 50  $\Omega$  for the original sets 2 and 3, as well as for the optimized parameter set.

**Table 9.** Parameter sets for simulation.

Set	$w$ , mm	$s$ , mm	$t$ , mm	$h$ , mm	$h_1$ , mm	$\epsilon_r$	$\epsilon_{r1}$
1	0.200	0.200	0.035	0.137	0.250	10.2	4.3
2	0.200	0.200	0.035	0.206	0.360	10.2	4.3
3	0.200	0.200	0.035	0.360	0.360	10.2	4.3
Optimized	0.260	0.200	0.135	0.200	0.400	10.2	4.3

The  $U_{\max}$  values for the structure with the original parameter sets 1, 2, and 3 after failures 1, 2, and 3 are summarized in Table S4. Figure 19 shows the  $U_{\max}$  values dependences for these parameter sets and switching options 1, 2, and 3 (from Table S4) on the failure number.

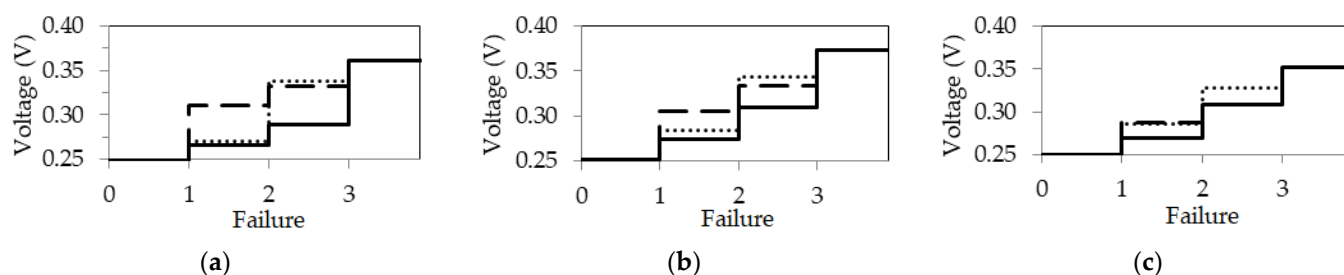


**Figure 19.** Dependences of  $U_{\max}$  for options 1 ( $\cdots$ ), 2 ( $---$ ), and 3 ( $—$ ) on the number of failures in the structure with the original parameter set (a) 1, (b) 2, and (c) 3.

Figure 19 shows that for switching options 1, 2, and 3, after failure 1 there was an increase in  $U_{\max}$  value to 0.27, 0.311, and 0.266 V; 0.284, 0.305, and 0.274 V; and 0.286, 0.287, and 0.269 V for original parameter sets 1, 2, and 3, respectively. After failure 2 it went up to 0.338, 0.332, and 0.289 V; 0.344, 0.333, and 0.309 V; and 0.328, 0.309, 0.308 V, respectively, and after failure 3 up to 0.361, 0.373, and 0.352 V, respectively. Switching option 3 is optimal, since the  $U_{\max}$  values after failures 1 and 2 were minimal (0.266 and 0.289 V; 0.274 and 0.309 V; and 0.269 and 0.308 V for original parameter sets 1, 2, and 3, respectively).

The  $U_{\max}$  values for the structure with an optimized parameter set after failures 1, 2, and 3 are summarized in Table S5. Figure 20 for switching options 1, 2, and 3 (from Table S5) shows the dependences of the  $U_{\max}$  values on the failure number.

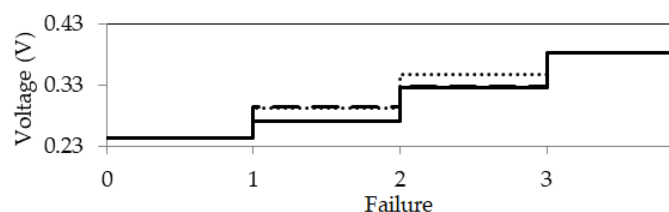


**Figure 20.** Dependences of  $U_{\max}$  values for options 1 ( $\cdots$ ), 2 ( $---$ ), and 3 ( $—$ ) on the failure number for the structure with the optimized parameter set.

Figure 20 shows that for options 1, 2, and 3 after failure 1, there was a change in  $U_{\max}$  value to 0.293, 0.294, and 0.271 V, respectively. After failure 2, it changed to 0.347 V, 0.328 V, and 0.327 V, respectively, and after failure 3 to 0.383 V. Switching option 3 is optimal since the  $U_{\max}$  values after failures 1 and 2 were minimal (0.271 and 0.327 V, respectively). Thus, for the structure with the optimized parameter set, the  $U_{\max}$  values after all failures are minimal and equal to 0.262, 0.287, and 0.334 V, respectively. As a result, in the structure

with the optimized parameters to failures, the  $U_{\max}$  value was minimal. However, after failure 3, it became the highest among all parameter sets.

The  $U_{\max}$  values for the optimal switching orders are summarized in Table 10. Figure 21 shows the  $U_{\max}$  dependences (from Table 10) on the failure number for the original parameter sets 1, 2, and 3 and the optimized parameter set.

Table 10.  $U_{\max}$  values for optimal switching orders.

Set	Before Failure	$U_{\max}$ , V	After Failure 1	$U_{\max}$ , V	After Failure 2	$U_{\max}$ , V	After Failure 3	$U_{\max}$ , V
1	R-R, R-R, R-R	0.248	R-R, R-R, R-SC	0.266	SC-R, R-R, R-SC	0.289	R-SC, OC-R, SC-R	0.361
2	R-R, R-R, R-R	0.252	R-R, R-R, R-SC	0.274	SC-R, R-R, R-SC	0.309	R-SC, OC-R, SC-R	0.373
3	R-R, R-R, R-R	0.250	R-R, R-R, R-SC	0.269	SC-R, R-R, R-SC	0.308	R-SC, OC-R, SC-R	0.352
Optimized	R-R, R-R, R-R	0.243	R-R, R-R, R-SC	0.271	SC-R, R-R, R-SC	0.327	R-SC, OC-R, SC-R	0.383

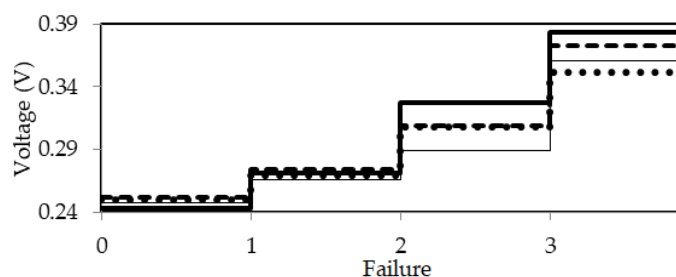


Figure 21. Dependences of  $U_{\max}$  values on the failure number for the structure with the original 1 (—), 2 (---), 3 (····), and optimized (— · —) parameter sets.

Figure 21 shows that with the optimal switching orders after failure 1, there was an increase in the  $U_{\max}$  value to 0.266, 0.274, and 0.269 (for the original parameter sets 1, 2, and 3, respectively) and 0.271 V (for the optimized parameter set). After failure 2, it increased up to 0.289, 0.309, 0.308, and 0.327 V, respectively, and after failure 3 up to 0.361, 0.373, 0.352, and 0.383 V, respectively. Thus, for the structure with the original parameter set 1, the  $U_{\max}$  values after failures 1 and 2 were minimal and equal to 0.266 and 0.289 V, respectively; however, after failure 3, the minimum  $U_{\max}$  value was for the structure with parameter set 3 (0.352 V). For all parameter sets, switching option 3 is optimal. As a result, parameter sets 1 and 3 are more preferable since they give lower  $U_{\max}$  values.

#### 4.5. Structure with the Reference Conductor in the Form of Side Polygons

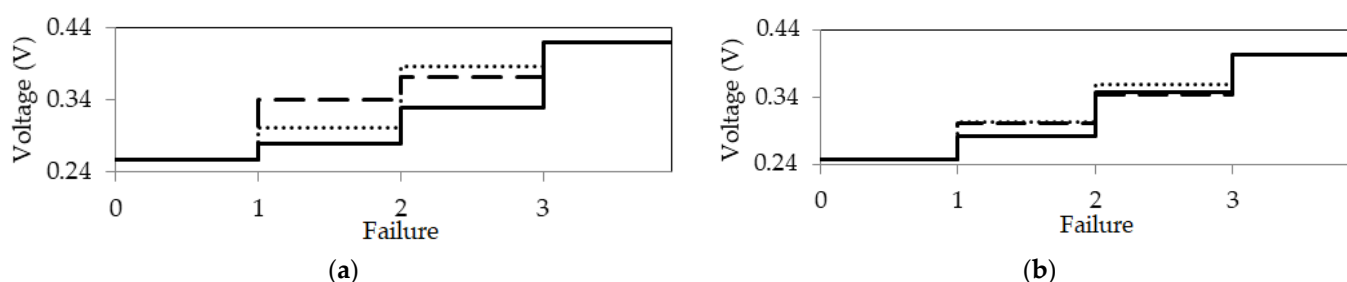
A cross-section for simulating a triple MR structure with the reference conductor in the form of side polygons is shown in Figure 1d. The original and optimized cross-section parameter sets were used for the simulation (Table 11). The  $R$  values (before failures) were equal to 50  $\Omega$  for the original parameter set and 105  $\Omega$  for the optimized one for the structure before failures.

Table 11. Parameter sets for simulation.

Set	$w$ , mm	$w_1$ , mm	$s$ , mm	$t$ , mm	$h$ , mm	$\epsilon_r$	$d$ , mm
Original	1.6	1.6	0.51	0.018	0.5	4.5	1.6
Optimized	0.5	1.6	0.22	0.018	0.3	4.5	8

The  $U_{\max}$  values for structures with the original and optimized parameter sets after failures 1, 2, and 3 are summarized in Table S6. Figure 22 shows the dependences of  $U_{\max}$

values on the failure number for these structures for switching options 1, 2, and 3 (from Table S6).



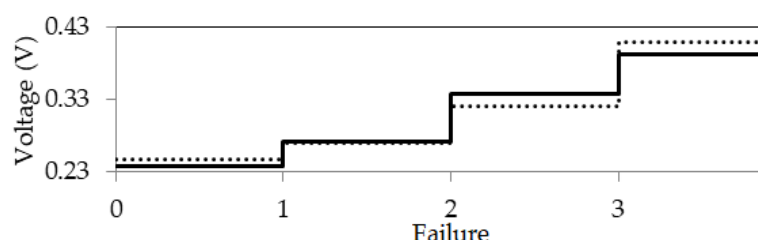
**Figure 22.** Dependences of  $U_{\max}$  on the failure number for options 1 ( $\cdots$ ), 2 ( $---$ ), and 3 ( $—$ ) for the structure with (a) original and (b) optimized parameter sets.

Figure 22a shows that for the structure with the original parameter set, with switching options 1, 2, and 3, after failure 1 the  $U_{\max}$  value increased to 0.292, 0.33, and 0.27 V, respectively; after failure 2 to 0.377, 0.362, and 0.32 V, respectively, and after failure 3 up to 0.409 V. Switching option 3 is optimal since the  $U_{\max}$  values after failures 1 and 2 in this case were minimal (0.27 and 0.32 V, respectively).

Figure 22b shows that for the structure with the optimized parameter set, with switching options 1, 2, and 3, after failure 1 there was a change in the  $U_{\max}$  value to 0.293, 0.291, and 0.272 V, respectively. After failure 2, it changed to 0.35, 0.334, and 0.337 V, respectively, and after failure 3 to 0.393 V. Switching option 3 is optimal since the  $U_{\max}$  value after failure 1 was 0.272 V, and after failure 2 was 0.337 V (differing from switching option 2 after failure 2 only by 0.003 V). The  $U_{\max}$  values for optimal switching orders are summarized in Table 12. Figure 23 shows the dependences of  $U_{\max}$  values (from Table 12) on failures for the original and optimized parameter sets.

**Table 12.**  $U_{\max}$  values for optimal switching orders.

Set	Before Failure	$U_{\max}$ , V	After Failure 1	$U_{\max}$ , V	After Failure 2	$U_{\max}$ , V	After Failure 3	$U_{\max}$ , V
Original	R-R, R-R, R-R	0.247	R-R, R-R, R-SC	0.270	OC-R, R-R, R-SC	0.320	R-SC, OC-R, SC-R	0.409
Optimized	R-R, R-R, R-R	0.237	R-R, R-R, R-SC	0.272	SC-R, R-R, R-SC	0.337	R-SC, OC-R, SC-R	0.393



**Figure 23.** Dependences of  $U_{\max}$  values on the failure number for the structure with the original ( $\cdots$ ) and optimized ( $—$ ) parameter sets.

Figure 23 shows that with the optimal switching orders after failure 1, there was an increase in  $U_{\max}$  values up to 0.27 (for the original parameter set) and 0.272 V (for the optimized parameter set). After failure 2, the increase went up to 0.32 and 0.337 V, respectively, and after failure 3 up to 0.409 and 0.393 V, respectively. Thus, for the structure with the optimized parameter set, the  $U_{\max}$  values after failure 3 were minimal and equal

to 0.393 V. However, if we consider failures 1 and 2, then the  $U_{\max}$  values were minimal for the structure with the original parameter set and were 0.27 and 0.32 V, respectively.

## 5. Discussion

A preliminary comprehensive study of structures with a reference conductor in the center, around, above and below, and in the form of side polygons was carried out. As a result of simulating the structures in different parameter ranges, it was revealed that the deviations of the  $U_{\max}$ ,  $\Delta f$ , and  $f_1$  values were insignificant. However, for the structure with a reference conductor around, there were deviations in the output signal waveforms (in time and frequency responses) and in the  $\Delta f$  and  $f_1$  values for different parameter sets. The attenuation of the exciting USP (relative to the input) was achieved for each structure by 4.04, 2.01, 3.98, and 4.18 times, respectively.

As a result of optimization by heuristic search, it was possible to equalize the time intervals between the decomposition pulses for structures with a reference conductor in the center, above and below, and as side polygons. In addition, it was possible to reduce the output voltage for structures with a reference conductor around (from 0.5 to 0.29 V), on the top and bottom (from 0.25 to 0.24 V), and as side polygons (from 0.243 to 0.235 V). For the structure with a reference conductor in the center, this value did not change because pairwise equalization of the pulse amplitudes was deliberately achieved by means of the structure symmetry.

The optimal switching orders for these structures with the original and optimized parameter sets were studied in detail:

1. For the structure with a reference conductor in the center, for both parameter sets, the optimal switching option was 3, and after all failures, the minimum  $U_{\max}$  values were obtained in the structure with the optimized parameter set (0.262, 0.287, 0.334 V), which makes it the most preferable.
2. For the structure with a reference conductor around, after failures 1, 2, and 3, the minimum  $U_{\max}$  values (0.502, 0.505, and 0.517 V, respectively) were observed with the original parameter set. The optimal switching order for the structure with the original parameter set was option 2. For the optimized parameter set, option 3 was optimal since the  $U_{\max}$  values were minimal (0.507, 0.527, and 0.718 V, respectively), but they were higher than with the original parameter set. Thus, the structure with the original parameter set is the most preferable in this case.
3. For the structure with a reference conductor above and below, after failures 1 and 2, the minimum  $U_{\max}$  values (0.266 and 0.289 V, respectively) were observed with parameter set 1, and after failure 3 with parameter set 3. For all parameter sets, option 3 was optimal. More preferably, there can be a structure with the original parameter set 1 with the minimum  $U_{\max}$  values after failures 1 and 2 (0.266 and 0.289 V, respectively).
4. For the structure with a reference conductor in the form of side polygons with the original and optimized parameter sets, option 3 was optimal. With the optimized parameter set, the  $U_{\max}$  value after failure 3 for all switching options was minimal and equal to 0.393 V. However, if we consider failures 1 and 2, then the  $U_{\max}$  values were minimal for the original parameter set and were 0.27 and 0.32 V, respectively. More preferable may be the structure with the original parameter set with the minimum  $U_{\max}$  values after failures 1 and 2 (0.27 and 0.32 V, respectively).

Based on the analysis of the data obtained, it can be concluded that the implementation of new devices with a triple MR is expedient for all the structures considered. However, for the structure with a reference conductor in the center, it is better to use the optimized parameter set. At the same time, for the structures with a reference conductor around, above and below, and as side polygons, the original one is best. The possibility of creating these structures is justified by the feasibility of structural and technological implementation.



## 6. Conclusions

For the first time, systematically (on four structures, with the original and optimized parameter sets), two new effects of asymmetry in initially symmetric structures with triple MR were investigated. First, the influence of asymmetry caused by the geometric parameter variations on per-unit length mode delays and time and frequency responses of the structures was shown. This allowed us to make useful quantitative estimates, showing, in general, a slight deterioration in MR effectiveness. Then, the successively increasing influence of the boundary conditions asymmetry caused by successive failures (SC or OC) was investigated. The evaluation of the sequential deterioration in the MR effectiveness that was carried out revealed the possibility of choosing the optimal order of switching the reserved circuits. It ensures the minimum deterioration without any costs for the implementation of such an order.

This study is remarkable due to its use of a simple but highly efficient method in which EMC is ensured only through reserving circuits, rather than widely used additional costly measures (such as protective devices or filters). The main difference between the investigated structures with triple MR and similar ones (for example, structures with single MR, which were more commonly studied earlier) is the fact that the problem of specifying the optimal switching order in those structures does not arise at all. Finally, the novelty of the performed research is clearly expressed in finding the optimal switching order of circuits after failure. This contributes to a highly effective way to maintain the protective characteristics of a structure. Meanwhile, the practical implementation does not require any costs.

In the future, we are planning to investigate structures with a triple MR in which failures are manifested not at the ends but along the conductors (a task that has never been posed before). In addition, next year it is planned to develop layouts, and to manufacture and measure the proposed structures. Finally, the authors are planning to investigate other asymmetry effects.

**Supplementary Materials:** The following are available online at <https://www.mdpi.com/article/10.3390/sym13061074/s1>, Table S1:  $U_{\max}$  values at the end of an active conductor after various failures for the structure with the original and optimized (sequentially) parameter sets, Table S2:  $U_{\max}$  values at the end of an active conductor after various failures for the structure with the original parameter set, Table S3:  $U_{\max}$  values at the end of an active conductor after various failures for the structure with the optimized parameter set, Table S4:  $U_{\max}$  values at the end of an active conductor after various failures for the structure with parameter sets 1, 2, 3, Table S5:  $U_{\max}$  values at the end of an active conductor after various failures for the structure with the optimized parameter set, Table S6:  $U_{\max}$  values at the end of an active conductor after various failures for the structure with the original and optimized parameter sets.

**Author Contributions:** Conceptualization, T.R.G.; validation, A.M.Z.; formal analysis, A.M.Z.; investigation, A.O.B., A.V.M., and E.B.C.; writing—original draft preparation, A.O.B., A.V.M., and E.B.C.; writing—review and editing, A.O.B. and T.R.G.; supervision, T.R.G. and A.M.Z. All authors have read and agreed to the published version of the manuscript.

**Funding:** The reported study was funded by the Russian Science Foundation, project number 20-19-00446, and RFBR, project number 19-37-51017.

**Institutional Review Board Statement:** Not applicable.

**Informed Consent Statement:** Not applicable.

**Data Availability Statement:** Not applicable.

**Acknowledgments:** The authors sincerely appreciate all valuable comments and suggestions from the reviewers, which helped us to improve the quality of the paper.

**Conflicts of Interest:** The authors declare no conflict of interest.

## References

1. Kapur, K.C.; Pecht, M. *Reliability Engineering*; Wiley: Hoboken, NJ, USA, 2014.
2. Li, Y.; Chen, H.; Huang, J.; Li, X.; Zhang, T.-Y.; Huang, H.-Z. Reliability Allocation and Prediction for Command and Control System. In Proceedings of the 2020 Global Reliability and Prognostics and Health Management (PHM-Shanghai), Shanghai, China, 16–18 October 2020; pp. 1–6.
3. Jin, T. *Reliability Engineering and Service*; Wiley: Hoboken, NJ, USA, 2019.
4. Ismail, E.; Utelieva, N.; Balmaganbetova, A.; Tursynbayeva, S. The choice of measures reliability of the software for space applications. In Proceedings of the 2020 International Conference on Electrical, Communication, and Computer Engineering (ICECCE), Istanbul, Turkey, 12–13 June 2020; pp. 1–5.
5. Öner, K.B.; Scheller-Wolf, A.; van Houtum, G.-J. Redundancy Optimization for Critical Components in High-Availability Technical Systems. *Oper. Res.* **2013**, *61*, 244–264. [\[CrossRef\]](#)
6. Van Acker, T.; Van Hertem, D. Redundancy Dependence in the Context of Competing Risks and Dynamic Degradation. *IEEE Trans. Reliab.* **2020**, *70*, 1–9. [\[CrossRef\]](#)
7. International Electrotechnical Commission. *IEC 60050-192 International Electrotechnical Vocabulary; Part 192: Dependability*; IEC: London, UK, 2015.
8. Fukatani, T.; Le, H.H.; Yokota, H. Lightweight Dynamic Redundancy Control for Server-Based Storage. In Proceedings of the 2019 38th Symposium on Reliable Distributed Systems (SRDS), Lyon, France, 1–4 October 2019; pp. 295–29509.
9. Kučera, M.; Šebök, M. Electromagnetic compatibility analysing of electrical equipment. In Proceedings of the 2016 Diagnostic of Electrical Machines and Insulating Systems in Electrical Engineering (DEMISEE), Papradno, Slovakia, 20–22 June 2016; pp. 104–109.
10. Radasky, W.A.; Hoad, R. Recent Developments in High Power EM (HPEM) Standards with Emphasis on High Altitude Electromagnetic Pulse (HEMP) and Intentional Electromagnetic Interference (IEMI). *IEEE Lett. Electromagn. Compat. Pract. Appl.* **2020**, *2*, 62–66. [\[CrossRef\]](#)
11. Hoad, R.; Radasky, W.A. Progress in High-Altitude Electromagnetic Pulse (HEMP) Standardization. *IEEE Trans. Electromagn. Compat.* **2013**, *55*, 532–538. [\[CrossRef\]](#)
12. Gaynutdinov, R.; Chermoshencev, S. Virtual Testing of Electronic Systems Susceptibility by Electromagnetic Compatibility Requirements. In Proceedings of the 2018 International Russian Automation Conference (RusAutoCon), Sochi, Russia, 9–16 September 2018; pp. 1–5.
13. Radasky, W.A. Introduction to the Special Issue on High-Altitude Electromagnetic Pulse (HEMP). *IEEE Trans. Electromagn. Compat.* **2013**, *55*, 410–411. [\[CrossRef\]](#)
14. Li, K.-J.; Xie, Y.-Z.; Zhang, F.; Chen, Y.-H. Statistical Inference of Serial Communication Errors Caused by Repetitive Electromagnetic Disturbances. *IEEE Trans. Electromagn. Compat.* **2020**, *62*, 1160–1168. [\[CrossRef\]](#)
15. Radasky, W.; Baum, C.; Wik, M. Introduction to the Special Issue on High-Power Electromagnetics (HPEM) and Intentional Electromagnetic Interference (IEMI). *IEEE Trans. Electromagn. Compat.* **2004**, *46*, 314–321. [\[CrossRef\]](#)
16. Gizatullin, Z.M.; Gizatullin, R.M.; Nuriev, M.G. Prediction of Noise Immunity of Computing Equipment under the Influence of Electromagnetic Interference through the Metal Structures of Building by Physical Modeling. In Proceedings of the 2020 IEEE Conference of Russian Young Researchers in Electrical and Electronic Engineering (EIConRus), St. Petersburg and Moscow, Russia, 27–30 January 2020; pp. 120–123.
17. Shkinderov, M.; Gizatullin, Z. Technique for Noise Immunity Analysis of Access Control Systems Using Electromagnetic Topology Method. In Proceedings of the 2020 International Russian Automation Conference (RusAutoCon), Sochi, Russia, 6–12 September 2020; pp. 144–148.
18. Belousov, A.O.; Chernikova, E.B.; Samoylichenko, M.A.; Medvedev, A.V.; Nosov, A.V.; Gazizov, T.R.; Zabolotsky, A.M. From Symmetry to Asymmetry: The Use of Additional Pulses to Improve Protection against Ultrashort Pulses Based on Modal Filtration. *Symmetry* **2020**, *12*, 1117. [\[CrossRef\]](#)
19. Pissort, D.; Lannoo, J.; Van Waes, J.; Degraeve, A.; Boydens, J. Techniques and measures to achieve EMI resilience in mission- or safety-critical systems. *IEEE Electromagn. Compat. Mag.* **2017**, *6*, 107–114. [\[CrossRef\]](#)
20. Degraeve, A.; Pissort, D. Study of the effectiveness of spatially EM-diverse redundant systems under plane-wave illumination. In Proceedings of the 2016 Asia-Pacific International Symposium on Electromagnetic Compatibility (AP EMC), Shenzhen, China, 17–21 May 2016; Volume 1, pp. 211–213.
21. Degraeve, A.; Pissort, D. Study of the effectiveness of spatially EM-diverse redundant systems under reverberation room conditions. In Proceedings of the 2016 IEEE International Symposium on Electromagnetic Compatibility (EMC), Ottawa, ON, Canada, 25–29 July 2016; pp. 374–378.
22. Sharafutdinov, V.R.; Gazizov, T.R. Analysis of reservation methods based on modal filtration. *Syst. Control Commun. Secur.* **2019**, *3*, 117–144. (In Russian) [\[CrossRef\]](#)
23. Sagiyeva, I.Y.; Gazizov, T.R.; Kenzhegulova, Z.M.; Surovtsev, R.S. Modal filters based on a microstrip line with overhead conductors grounded at both ends. In Proceedings of the 22st International Conference of Young Specialists on Micro/Nanotechnologies and Electron Devices EDM, Erlagol, Russia, 30 June–4 July 2021; pp. 1–4, to be published.
24. Kuksenkov, S.P. Preliminary results of TUSUR University project for design of spacecraft power distribution network: EMC simulation. *IOP Conf. Ser. Mater. Sci. Eng.* **2019**, *560*, 1–7. [\[CrossRef\]](#)